

Article

Sliding Mode with Equivalent Control for Induction Motor Drive Based on Multi-Pulse VSC

Carlos E. Castañeda ¹, Antonio Valderrabano-Gonzalez ^{2,*}, Hossam A. Gabbar ³ and Onofre A. Morfín ⁴

- ¹ Centro Universitario de los Lagos, Universidad de Guadalajara, Lagos de Moreno 47460, Jalisco, Mexico; carlose.castanedah@academicos.udg.mx
- ² Facultad de Ingeniería, Universidad Panamericana, Álvaro del Portillo 49, Zapopan 45010, Jalisco, México
- ³ Faculty of Engineering and Applied Science, Ontario Tech University, Oshawa, ON L1G 0C5, Canada; hossam.gaber@ontariotechu.ca
- ⁴ Departamento de Eléctrica y Computación, Instituto de Ingeniería y Tecnología, Universidad Autónoma de Ciudad Juárez, Ciudad Juárez 32310, Chihuahua, Mexico; omorfin@uacj.mx
- * Correspondence: avalder@up.edu.mx

Abstract: In this work, the application of a sliding mode equivalent control for an induction motor drive based on a multi-pulse Voltage Source Converter is proposed. This is accomplished by transforming the squirrel-cage induction motor mathematical model into a block control form. The equivalent control method is applied to the sliding manifold, where the voltages are obtained in the stationary reference frame to control the angular velocity of the motor. In addition, a proportional-integral control is designed and applied to the motor represented in this form in order to make performance comparisons with the equivalent control method. Multi-pulse converters of 6, 12, and 84 pulses are used directly to feed the plant that is being controlled. The outcomes of using these power electronics devices are used to perform comparisons among the velocity tracking performance, control voltages in stationary reference frame, tracking errors, and rejection of external disturbances. Furthermore a dynamic and steady-state analysis of the velocity tracking performance is executed. The energy profiles for the startup, torque variations, and steady-state are also obtained. Additionally, total harmonic distortion values are added. All comparisons are carried out using the established plan for the motor, both with and without the use of power electronics converters, and with both control algorithms. The obtained results demonstrate that the use of a high-quality voltage source converter, along with a good control strategy, allows for a general improvement in the overall system and a significant reduction in energy usage, whilst also reducing controller complexity.

Keywords: multi-pulse VSC; equivalent control; sliding modes control



Citation: Castañeda, C.E.; Valderrabano-Gonzalez, A.; Gabbar, H.A.; Morfín, O.A. Sliding Mode with Equivalent Control for Induction Motor Drive Based on Multi-Pulse VSC. *Energies* **2023**, *16*, 4866. <https://doi.org/10.3390/en16134866>

Academic Editor: Gianluca Brando

Received: 4 May 2023
Revised: 7 June 2023
Accepted: 13 June 2023
Published: 22 June 2023



Copyright: © 2023 by the authors. Licensee MDPI, Basel, Switzerland. This article is an open access article distributed under the terms and conditions of the Creative Commons Attribution (CC BY) license (<https://creativecommons.org/licenses/by/4.0/>).

1. Introduction

Efficiently tracking the speed control of induction motors remains a challenging task, mainly due to its nonlinear dynamics and the reaction it might have with possible external disturbances. Anticipating any possible variation to the planned functioning and preventing it by using conventional control algorithms demands high effort because of the high-order of the mathematical model and the non-linearity. There are many advanced strategies, such as Active Disturbance Rejection Control [1], where parameter changes are compensated for by using the extended state observer and nonlinear state error feedback; Model Predictive Current Control (MPCC) [2], which uses a novel integral sliding mode observer and an adaptive observer to establish a robust prediction model for the stator current prediction; fast high-order terminal sliding mode (HO-TSM) current controller [3], which simultaneously obtains rapid convergence and effective chattering suppression, where a surface is designed based on the system state and the control law includes a linear integral term to enhance the capability of disturbance compensation. Furthermore, a

nonlinear gain leads to satisfactory chattering suppression during steady-state; a second-order terminal sliding mode (SO-TSM) speed controller [4] with nonlinear control gain can obtain strong torque rejection capability to suppress the speed fluctuation, where a manifold introduces the convergence trajectory without speed overshoot and the integral term control law compensates for the external disturbance with the anti-windup mechanism. An analytic tuning method is created for the boundary layer limit of the saturation function by means of an anti-windup integral sliding manifold [5] for the discrete-time pseudo-sliding mode control applied to the induction motor drives. The stator field-oriented control (SFOC) for induction motor drives with a sliding mode control and fuzzy logic control for speed recognition without requiring precise motor modeling [6], where the new nonlinear sliding surface design increases the efficiency of the controller and reduces the chattering effect, and finally, a third-order inverter is used to eliminate the high-order harmonics components on the load current. A robust input-output feedback linearization control technique is proposed for induction motors in which the controller is designed to be robust against variations in the stator and rotor resistances [7]. It also accounts for the magnetizing inductance, ensuring correct behavior and offering optimal dynamic performance in all working conditions. The controller is capable of coping with the uncertainties of the model. Four sensorless control schemes for the operation of induction motors in the field-weakening region are compared and assessed in terms of performance and complexity [8]. The first one is the control scheme of a stator-flux-oriented drive, and the three other controllers are the control schemes of rotor-flux-oriented drives. The control schemes analyze the motor voltage to adjust the flux level. A H_∞ linear parameter varying (LPV) approach to speed control of induction motor drives has been proposed [9]. The robust controller is designed based on the hybrid current-flux d - q equations of the induction motor mode, where the rotor speed is used as a scheduling variable, and the resulting control is a sum of the weighted control efforts, which depend on the current value. Takagi-Sugeno fuzzy logic controllers [10], have been employed, replacing the Proportional-Integral (PI) controller with a fuzzy logic controller. This approach evaluates the flux and torque in a cost function to generate an optimal inverter switching state within a sampling period. Adaptive Neuronal controllers [11] utilize B-spline artificial neural networks for online parameter adjustment. This approach has been used to improve the dynamic properties of the control system and has achieved good results. Most of these researches use the motor drive as a black box with the possibility of providing any level of voltage and frequency. An essential part of the drive system is the Voltage Source Converter (VSC), which is responsible for changing the nature of the voltage to ensure that the speed of the motor is tracking the planned trajectory, and a reduced Total Harmonic Distortion (THD) is produced. A low quality VSC might degrade the overall functioning of the system and add more complexity to the controller design. In addition, energy used for starting up and managing any variation in the motor speed can be high even in a short period of time. On the other hand, it is well known that the sliding mode control algorithm, particularly the equivalent control results, is a great strategy for controlling nonlinear systems and is also very robust to external disturbances [12,13]. There are different ways to design the sliding manifold, with one of them being the very well-known transformation of the nonlinear system to be controlled, which is used to block the control form [14,15]. This strategy is very effective because the last block of the transformation constitutes the sliding manifold and is therefore ready to apply the equivalent control method. This paper presents a sliding mode with the equivalent control in conjunction with voltage source converters of 6, 12, and 84 pulses.

The main contribution of this work is to show the advantages of applying a Voltage Source Converter of 84 pulses over the use of the standard converters of 6 and 12 pulses when a defined task is established through a control system. The quality of the signals provided by power electronics converters may result in a different performance than what is expected. The use of the 84 pulses converter ensures a THD lower than 3%, which results in a very low variation in comparison to the developed plan.

This work is organized as follows: Section 2 presents the background of the 6, 12, and 84 pulse converters. Section 3 presents the control design based on the mathematical model of the squirrel cage induction motor. Based on this model, a transformation to the block control form is performed, resulting in the sliding manifold. The equivalent strategy and PI control strategies are then applied. Section 4 depicts the experiment design where the conditions of the simulations are illustrated. The results of the simulations are shown in Section 5, and the conclusions and discussion of the results are presented in Sections 6 and 7, respectively.

2. Multi-Pulse Converters

Multi-pulse converters refer to the type of DC to AC inverters that split the output signal into parts of the same width (pulses), providing the concept of a timed pulsation. By combining this timed pulsation with different amplitudes we can achieve a stepped signal very close to a sinusoidal one. The greater the number of divisions within the period of a signal, each with different associated amplitudes, the better the shape of the output. Conventional multi-pulse converters are designed with 6 and 12 pulses, but some researchers have demonstrated that by using neutral point re-injection, an effect of pulse multiplication can be obtained [11,16,17], resulting in harmonic content reduction.

2.1. The 6- and 12-Multi-Pulse Converters

The 6-pulse converter is considered to be the basic cell for converting DC to AC signals. It is also known as a two-level converter that can bring an output of three levels when it is connected in a wye configuration. By adding two 6-pulse converters (wye and delta connection), and performing the required angle and amplitude corrections as indicated in Ref. [18], a 12-pulse converter is configured. These 6-pulse and 12-pulse converters have been used in many medium and high-power applications where stringent power quality is not required or with the use of a power filter to ensure that high distortion is not generated. If no power filter is used with these converters, the applications are limited according to international standards [19,20], but in many cases, they are still being used, ignoring the cited recommendations. This research highlights some disadvantages of using non-filtered 6- and 12-pulse converters, as opposed to using 84-pulse converter, which has a voltage output with a total harmonic distortion lower than 3%. The similarities obtained with the last converter in comparison with the ideal signal matches that required by the induction motor to develop a defined task.

2.2. The 84-Multi-Pulse Converter

There is a noticeable difference in the 12-pulse converter used for re-injection through the neutral point, as the DC source is not shared between the 6-pulse modules. The positive multi-pulse signal between the main terminals of the first 6-pulse converter and the mirrored positive multi-pulse signal to the second 6-pulse converter are connected. To achieve a neutral point, the negative terminal of the first converter is connected to the positive terminal of the second converter. With this slight modification, a neutral point re-injection can be obtained with the effect of pulse number multiplication. We have used a 7-level inverter as the pulse generator to obtain 84 pulses, as depicted in Figure 1 [21].

The process of synchronizing and tracking the required amplitude of three-phase voltage to ensure the motor performance is not considered a part of this research, but interested readers can refer to Refs. [11,18]. The aim of this research is to contrast the use of three different voltage source converters for the velocity control of an induction motor. The advantages of using a generated signal that is very close to the required one are presented by the following illustrations and tables.

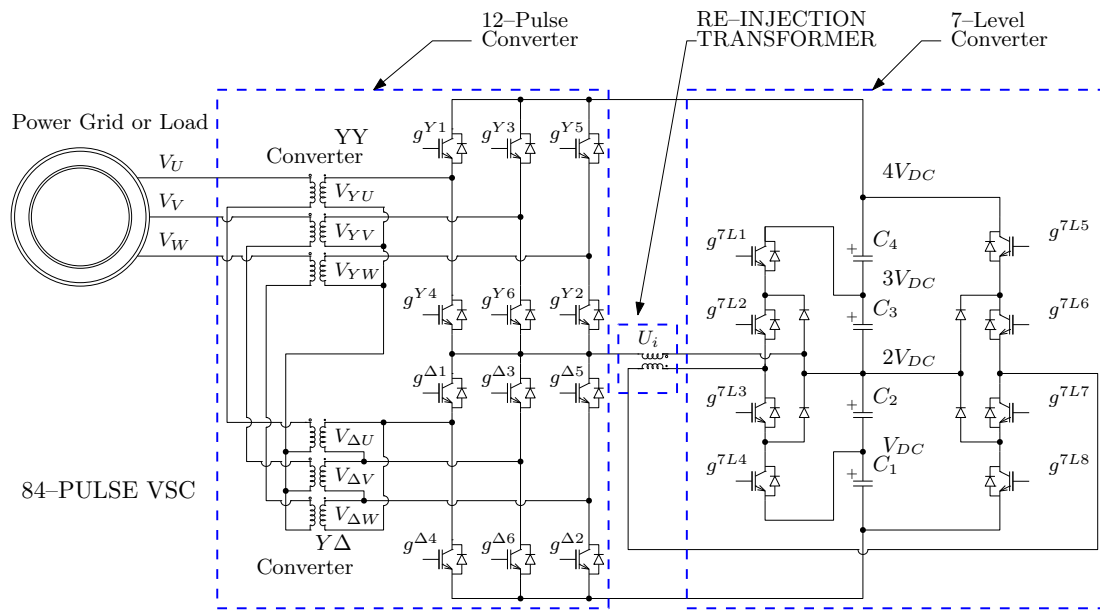


Figure 1. The 84-pulse voltage source converter.

3. Control Design

The mathematical model of the squirrel-cage induction motor in the α - β axes, transformed into the stationary reference frame, is as follows [14,22]:

$$\begin{aligned}
 \frac{d\omega_m}{dt} &= K_T (i_{\beta s} \lambda_{\alpha r} - i_{\alpha s} \lambda_{\beta r}) - \frac{B_m}{J_m} \omega_m - \frac{1}{J_m} T_L \\
 \frac{d\lambda_{\alpha r}}{dt} &= -\frac{1}{T_r} \lambda_{\alpha r} - \frac{P}{2} \omega_m \lambda_{\beta r} + \frac{L_m}{T_r} i_{\alpha s} \\
 \frac{d\lambda_{\beta r}}{dt} &= \frac{P}{2} \omega_m \lambda_{\alpha r} - \frac{1}{T_r} \lambda_{\beta r} + \frac{L_m}{T_r} i_{\beta s} \\
 \frac{di_{\alpha s}}{dt} &= \frac{\delta}{T_r} \lambda_{\alpha r} + \frac{P}{2} \delta \omega_m \lambda_{\beta r} - \gamma i_{\alpha s} + \frac{1}{\sigma L_s} v_{\alpha s} \\
 \frac{di_{\beta s}}{dt} &= -\frac{P}{2} \delta \omega_m \lambda_{\alpha r} + \frac{\delta}{T_r} \lambda_{\beta r} - \gamma i_{\beta s} + \frac{1}{\sigma L_s} v_{\beta s}
 \end{aligned} \tag{1}$$

where ω_m is the angular mechanical velocity; $\lambda_{\alpha r}$ and $\lambda_{\beta r}$ are the rotor flux linkages at α and β axis, respectively; $i_{\alpha s}$ and $i_{\beta s}$ are the stator currents, and $v_{\alpha s}$ and $v_{\beta s}$ are the control inputs. The definitions of the remaining parameters and parameter constants of the induction motor model (1) can be found in Refs. [14,22]. Then, in order to create a sliding manifold, the system (1) is transformed in the following block control form based on the error variables:

$$\begin{aligned}
 \dot{\epsilon}_1 &= -K_1 \epsilon_1 + \begin{bmatrix} K_T \lambda_r^\top M \\ 2 \frac{L_m}{T_r} \lambda_r^\top \end{bmatrix} \epsilon_2 \\
 \dot{\epsilon}_2 &= F(\lambda_r, \epsilon_1, \epsilon_2) - B_2 v_s \\
 \dot{\lambda}_{\alpha r} &= -\frac{1}{T_r} \lambda_{\alpha r} - \frac{P}{2} (\omega_{ref} - \epsilon_\omega) \lambda_{\beta r} + \frac{L_m}{T_r} i_{\alpha s}
 \end{aligned} \tag{2}$$

For simplicity, the procedure of transformation is not shown, and the reader is kindly referred to Ref. [14]. The last equation of system (2) is used to complete the order of

the system. Then, the new state variables of system (2) are: $\varepsilon_1 = \begin{bmatrix} \omega_{ref} - \omega_m \\ \phi_{ref} - \phi_r \end{bmatrix}$, and $\varepsilon_2 = \begin{bmatrix} \dot{i}_{ref} - \dot{i}_s \end{bmatrix}$, where:

$$\dot{i}_{ref} = \begin{bmatrix} K_T \lambda_r^\top M \\ 2 \frac{L_m}{T_r} \lambda_r^\top \end{bmatrix}^\top \left\{ \begin{bmatrix} \dot{\omega}_{ref} + \frac{B_m}{J_m} \omega_m \\ \dot{\phi}_{ref} + \frac{2}{T_r} \phi_r \end{bmatrix} + \begin{bmatrix} \frac{1}{J_m} \dot{T}_L \\ 0 \end{bmatrix} + K_1 \varepsilon_1 \right\} \quad (3)$$

The sliding manifold is defined by using the error vector ε_2 of system (2) as:

$$s = \dot{i}_{ref} - \dot{i}_s \quad (4)$$

and whose dynamics are: $\dot{s} = F(\lambda_r, \varepsilon_1, \varepsilon_2) - B_2 v_s$, where:

$$F(\lambda_r, \varepsilon_1, \varepsilon_2) = \frac{d}{dt} \dot{i}_{ref} - \begin{bmatrix} \frac{\delta}{T_r} & \frac{P}{2} \delta (\omega_{ref} - \varepsilon_w) \\ -\frac{P}{2} \delta (\omega_{ref} - \varepsilon_w) & \frac{\delta}{T_r} \end{bmatrix} \lambda_r + \gamma (\dot{i}_{ref} - \varepsilon_2) \quad (5)$$

and $B_2 = \begin{bmatrix} \frac{1}{\sigma L_s} & 0 \\ 0 & \frac{1}{\sigma L_s} \end{bmatrix}$. Then, with a feasible control input $v_s = [v_{\alpha s} \ v_{\beta s}]^\top$, the movement of the manifold $s = \varepsilon_2$ is forced to zero in finite time, and the stator current vector achieves \dot{i}_{ref} and the dynamics $\dot{\varepsilon}_2$ set the asymptotic movement towards the origin of the tracking error variable ε_1 . Based on the block control transformation (2), in this work, two control algorithms are proposed in order to obtain the control input vector v_s to control the angular velocity of the squirrel-cage induction motor model (1), which are explained in the following subsections.

The remaining parameters of system (2) can be found in Ref. [14]. The procedure for transforming a nonlinear system (in our case system (1)), to the desired block control form (the resulting form (2)), is explained in Ref. [23].

3.1. Sliding Modes with Equivalent Control

In this work we used the well-known sliding modes with the equivalent control method [12], where the sliding manifold is designed by using the transformation of the non-linear system to be controlled (1) to the block control form (2).

As was previously explained, the error vector ε_2 of system (2) constitutes the sliding mode (4), such that $s = \varepsilon_2 = 0$. Then, taking into account the control bound u_{max} as the maximum voltage given by the source, and by applying the following equivalent control [12]:

$$u = \begin{cases} u_{eq} & \text{if } \|u_{eq}\| \leq u_{max} \\ \frac{u_{max} u_{eq}}{\|u_{eq}\|} & \text{if } \|u_{eq}\| > u_{max} \end{cases} \quad (6)$$

giving $\dot{\varepsilon}_2 = 0$ of system (2), then $u_{eq} = B_2^{-1}[F(\lambda_r, \varepsilon_1, \varepsilon_2)]$; thus, the control signal u (6) makes the tracking error converge to a vicinity of the sliding manifold $s = 0$. For a more detailed explanation regarding the existence conditions of the sliding mode with equivalent control, see Ref. [12].

3.2. PI Controller

The design of the PI controller is through the obtained block control form transformation (2) based on the error dynamics from system (1). For this, the chosen sliding manifold is defined as $\dot{s}_2 = \dot{z}_2$ of the transformation (2). Then, the PI controller is proposed as follows:

$$v_s = K_p s + K_i \int_0^\tau s \, d\tau \quad (7)$$

where K_p and K_i are the diagonal matrices that correspond to the proportional and integral gains, respectively. Then, in order to force the surface movement of the sliding manifold

s to zero, and to achieve i_{ref} , by setting a control system with the control action of v_s , the surface variable moves to zero in finite time, and then achieves its reference i_{ref} by setting a control system by currents. Consequently, the error vector ε_1 has an asymptotic movement to zero, in order to fulfill the control goal, which is to control the velocity motor and regulate the modulus of the rotor flux linkages.

4. Experimental Design

For this work, we have considered the following conditions for simulation: the angular velocity reference is $\omega_{ref} = 500$ rev/min; the values for the load torque (external disturbance) T_L are (see Figure 2 for reference):

- from 0 to 0.25 s, $T_L = 4$ N · m
- from 0.25 to 0.5 s, $T_L = 12$ N · m
- from 0.5 to 0.75 s, $T_L = 2$ N · m
- from 0.75 to 0.85 s, $T_L = 10$ N · m
- from 0.85 to 1 s, $T_L = 6$ N · m

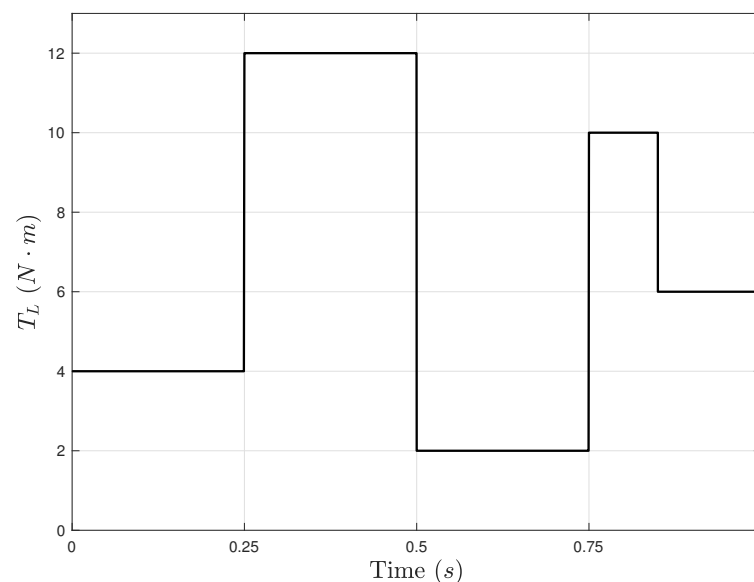


Figure 2. Load torque T_L .

These sudden changes of T_L (at 0.25, 0.5, 0.75, and 0.85 s) are used to verify the effectiveness of both controllers regarding the hard changes of the external disturbance and to make some statistical comparisons of the systems with and without VSC. The term “without VSC” means an ideal source able to provide any sinusoidal voltage at any frequency that corresponds to the control inputs at the α - β stationary reference frame in the simulation of the induction motor velocity controller, where it is not necessary to condition the signals. The same conditions of angular velocity reference and the sudden changes in the load torque are applied to a system without VSC, and to systems with VSCs of 6, 12, and 84 pulses. The simulation is made using Simulink of MATLAB[®] Version 2022b, and using PLECS[®] module Version 4.6.8. The time simulation is 1×10^{-5} s, using the solver Ode3 (Bogacki-Sampine) type fixed-step. The induction motor model parameters used in the simulation are presented in Table 1 [24].

Table 1. Induction motor model parameters [24].

Parameter	Value	Units
Stator resistance, R_s	0.435	Ω
Rotor resistance, R_r	0.816	Ω
Stator leakage reactance, X_{ls}	0.754	Ω
Rotor leakage reactance, X_{lr}	0.754	Ω
Magnetizing reactance, X_M	26.13	Ω
Inertial moment, J_m	0.0890	$\text{kg} \cdot \text{m}^2$
Power, P	3	HP
Line-to-line rated voltage	220	V

The statistical analysis for the velocity tracking performance is made between systems with and without VSC, as shown in Table 2, and includes the following parameters:

- The transient response, which includes:
 - Maximum overshoot M_p (or in case, undershoot $M_{\bar{p}}$): the maximum peak value of the response curve.
 - Rise time t_r : the time required for the response to rise from 0 to 100%.
 - Peak time t_p : the time required for the response to reach the first peak of the overshoot.
 - Settling time t_s : the time required for the response curve to reach and stay within a range for the final value of size specified by the absolute percentage, which in this case is the value of 1%.
- The steady-state analysis is done using the root-mean-square (RMS) error, which is used as a measure of the differences between values predicted by a model or an estimator and the values observed. This analysis is applied when the effect of each change of disturbance disappears.

Table 2. Dynamical and steady-state analysis for the velocity tracking performance.

Time (s) Torque (N · m)	Parameter	No VSC		6 Pulses		12 Pulses		84 Pulses	
		SM	PI	SM	PI	SM	PI	SM	PI
0 4	M_p (%)	18.50	0	13.6	0	18.25	0	18.30	0
	t_r (s)	0.00705	0.0755	0.00848	0.08	0.0072	0.079	0.00719	0.077
	t_p (s)	0.00929	0.0755	0.01010	0.08	0.00946	0.079	0.00943	0.077
	t_s (s)	0.07026	0.071	0.5612	0.07214	0.0558	0.06912	0.05514	0.0685
	RMS error	0.2681	0.1435	4.3366	0.1546	0.2412	0.145	0.1797	0.1441
0.25	M_p (%)	0.162	0.036	1.1	0.029	0.15	0.034	0.126	0.032
12	RMS error	0.0726	0.0767	1.5977	0.0848	0.2137	0.0752	0.056	0.0749
0.5	M_p (%)	0.232	0.0382	0.396	0.056	0.238	0.048	0.236	0.048
2	RMS error	0.2541	0.0594	1.4208	0.0687	0.2847	0.0584	0.2227	0.0583
0.75	M_p (%)	0.152	0.062	0.384	0.074	0.136	0.074	0.130	0.068
10	RMS error	0.2597	0.0605	1.5136	0.0691	0.2954	0.0609	0.2187	0.0605
0.85	M_p (%)	0.108	0.01	0.460	0.016	0.114	0.0134	0.106	0.0132
10	RMS error	0.1726	0.0505	0.8073	0.0601	0.2256	0.0497	0.1378	0.0495

The transient analysis is applied at the beginning of the simulation (parameters M_p , t_r , t_p , and t_s) and at the immediate instant of time after each perturbation is changed (parameters M_p or in case $M_{\bar{p}}$). We use $M_{\bar{p}}$ when the change of the disturbance undergoes a transition from a larger value to a smaller one: at 0.5 s (from 12 to 2 N · m) and at 0.85 s (from 10 to 6 N · m). On the contrary, we employ M_p (0, 0.25, and 0.75 s).

5. Simulation Results

• Sliding modes with equivalent control

In order to present the effectiveness of the control algorithm along with the use of the power electronics converter, Figure 3 shows the velocity tracking performance for the squirrel-cage induction motor without VSC and with VSCs of 6, 12, and 84 pulses. In this figure, 1 s of simulation is depicted, and the effect of changes or disturbances in the torque are presented with ovals. In addition, the detail of each system to reach the reference ω_{ref} is shown from 0.225 to 0.25 s. It can be noted in the detail that the three signals are very similar with the exception of the ω_{rSM6} (VSC of 6 pulses). Note that in the time of 0.25 s when the torque changes from 4 to 12 N · m, there are variations on the signals of ω_{rSM} , ω_{rSM12} , and ω_{rSM84} , with minimum variations in the oscillation.

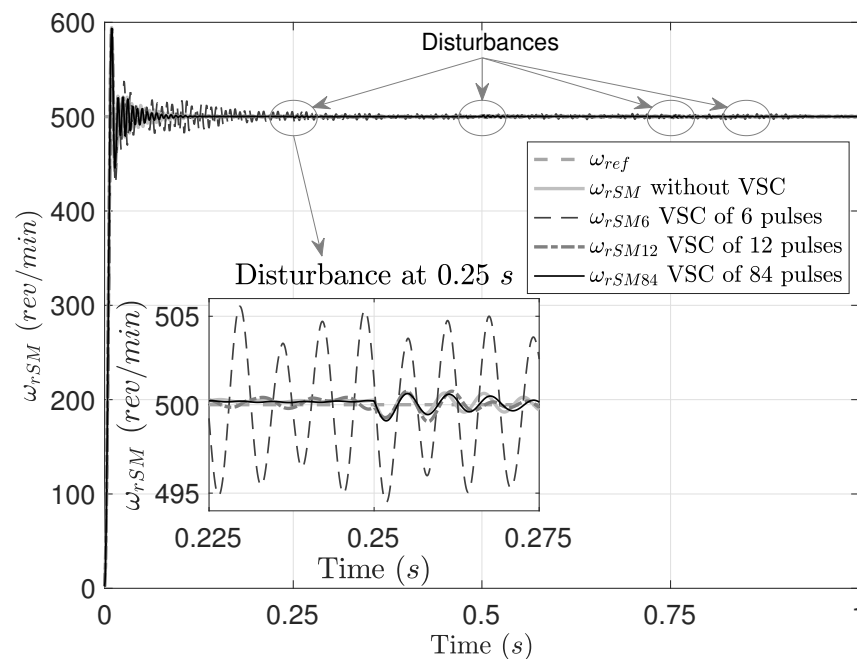


Figure 3. Velocity tracking performance for the squirrel-cage induction motor without VSC and with VSCs of 6, 12, and 84 pulses using sliding modes with the equivalent control algorithm.

The velocity tracking errors for squirrel cage induction motor without VSC and with VSCs of 6, 12, and 84 pulses are presented in Figure 4, where the convergence of each signal to zero can be seen with and without VSC. A detail is presented where it can be noted that at 0.25 s there are some oscillations due to the change of the external disturbance from 4 to 12 N · m. These oscillations have minimum differences in amplitude and phase, with the exception of ε_{rSM6} , which presents bigger oscillations than the other systems.

The control signals $v_{\alpha sSM}$ and $v_{\beta sSM}$ are presented in Figures 5 and 6, respectively. Here the voltages are displayed for systems with and without VSC. It can be noted that in both figures, the voltages $\|u_{eq}\|$ are applied at approximately 0.03 s, and after that the sliding manifold is reached. In addition, both figures shown a detailed view where a disturbance is presented from 4 to 12 N · m. It is observed that the signals change in amplitude when the disturbance is presented.

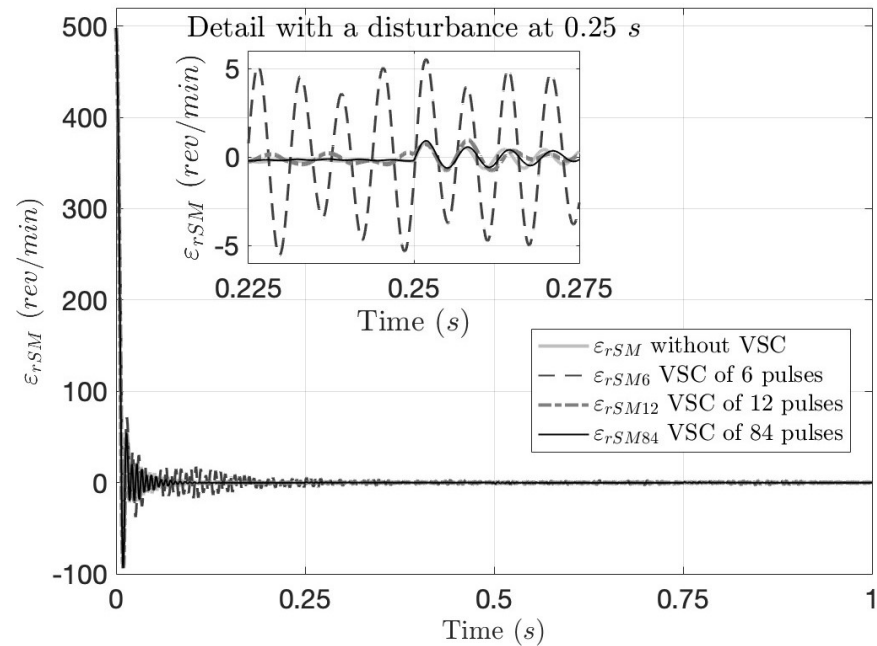


Figure 4. Tracking errors for squirrel cage induction motor without VSC and with VSCs of 6, 12, and 84 pulses using sliding modes with the equivalent control algorithm.

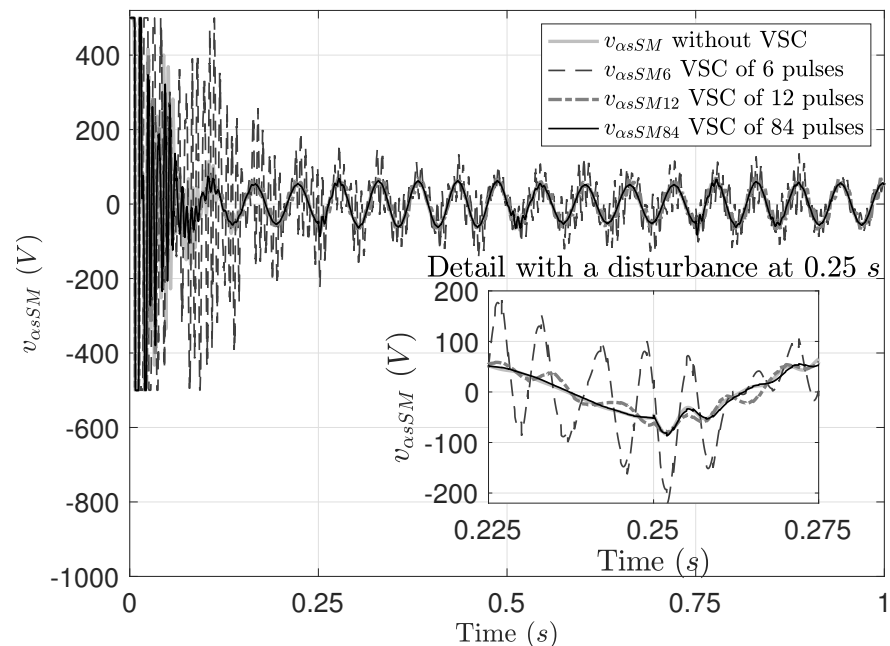


Figure 5. Control input performance $v_{\alpha sSM}$ using sliding modes with the equivalent control algorithm.

The velocity of the motor and torque variations on the connected load demand higher energy compared to that required for steady-state without any fluctuations. Considering a load that requires a constant velocity of 500 rev/min, an idle induction motor with the parameters of Table 1 and the torque variations indicated in Figure 2, the used energy profile of the motor is portrayed in Figure 7. The high energy needed to start up is evident and a slight slope can be noticed after the disturbances take place. Figure 8 presents the energy needed after startup and the perturbances end to illustrate the requirements of steady-state energy. The significance this is that the performance of the motor for the variations considered are fulfilled with an ideal VSC. This is the the basis for comparing different VSC structures and to define how to achieve the expected results in a better way.

The startup for the idle motor to achieve the required velocity considering the voltage required is generated with the ideal source (without VSC) is 1206.76 J. This is considered 100% of the energy used in 0.2 s. Using a 6-pulse VSC to generate the required voltage demands around 2.2 times the energy calculated for the startup. When a larger amount of pulses is used to build a VSC and drive the motor, the required amount of energy is slightly smaller than the ideal. The energy consumption is indicated in Table 3. As expected, an almost straight line is obtained and the slope indicates the energy consumption. The 84-pulse VSC exhibits the best performance and with the lowest amount of energy used. The frequency of the steady-state signal required for the system to function is 17.85714 Hz, with a maximum voltage of 54.3 V and 38.4117 V_{RMS} and the variations are illustrated in Figure 9. The total harmonic distortion (THD) is 0.09%, 2.84%, 34.24%, and 61.41% for outputs without VSCs, 84, 12, and 6 pulses, respectively.

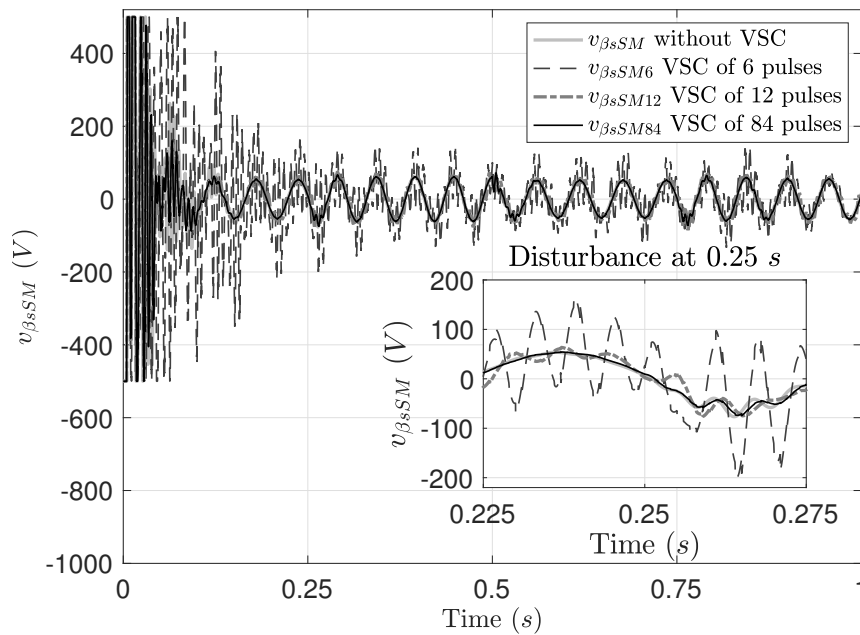


Figure 6. Control input performance $v_{\beta sSM}$ using sliding modes with the equivalent control algorithm.

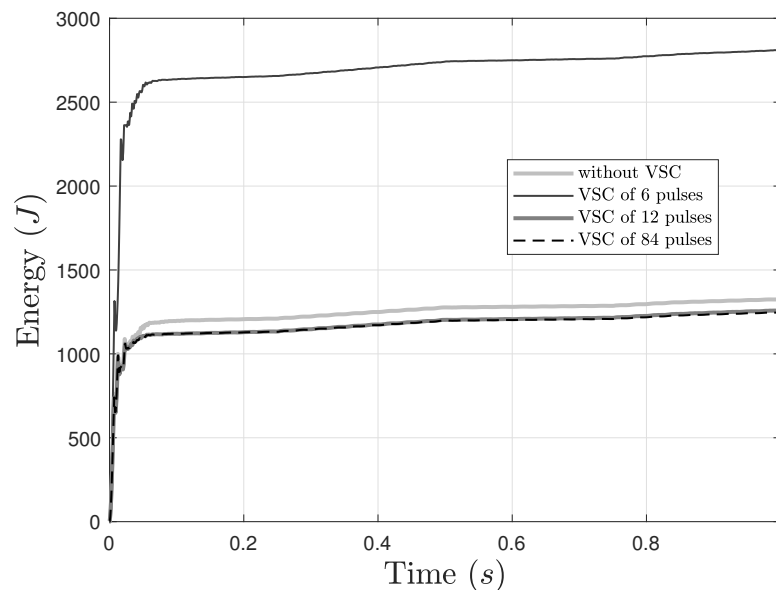


Figure 7. Energy profile for the squirrel cage induction motor without VSC and with VSCs of 6, 12, and 84 pulses using sliding modes with the equivalent control algorithm.

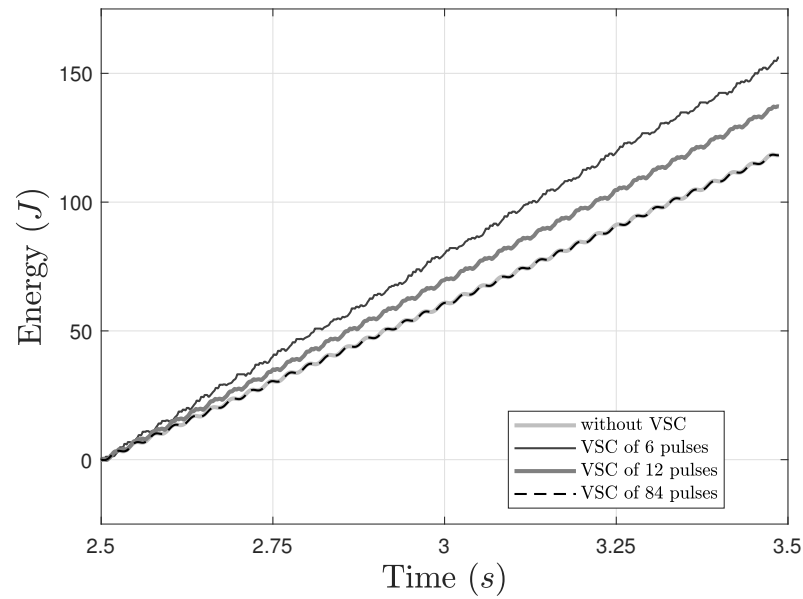


Figure 8. Energy profile for the squirrel cage induction motor without VSC and with VSCs of 6, 12, and 84 pulses, after torque variations using sliding modes with the equivalent control algorithm.

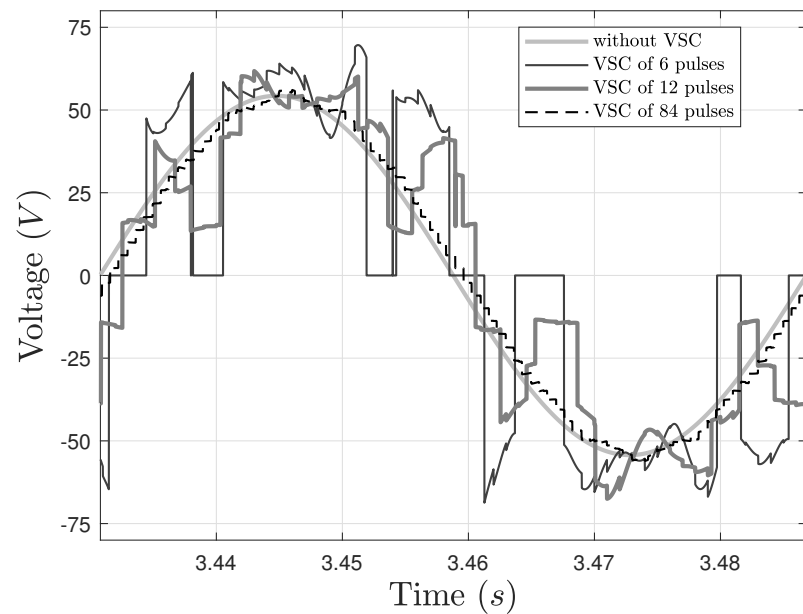


Figure 9. Steady state voltage without VSC and with VSCs of 6, 12, and 84 pulses using sliding modes with the equivalent control algorithm.

- **PI controller**

Figure 10 presents the velocity tracking performance for the squirrel-cage induction motor without VSC and with VSCs of 6, 12, and 84 pulses using the PI control algorithm. The tracking is almost the same in all signals, with a little difference when using the VSC of 6 pulses. In addition, the detailed window shows the effect on the motor speed when a sudden change from 4 to 12 N · m takes place at 0.25 s. The behavior of the speed signals is also very similar. Additionally, Figure 11 shows the tracking errors on the speed for the squirrel cage induction motor without VSC and with VSCs of 6, 12, and 84 pulses using the PI control algorithm. In steady-state, all the signals are at zero or very close to zero, which can be confirmed in the detailed view.

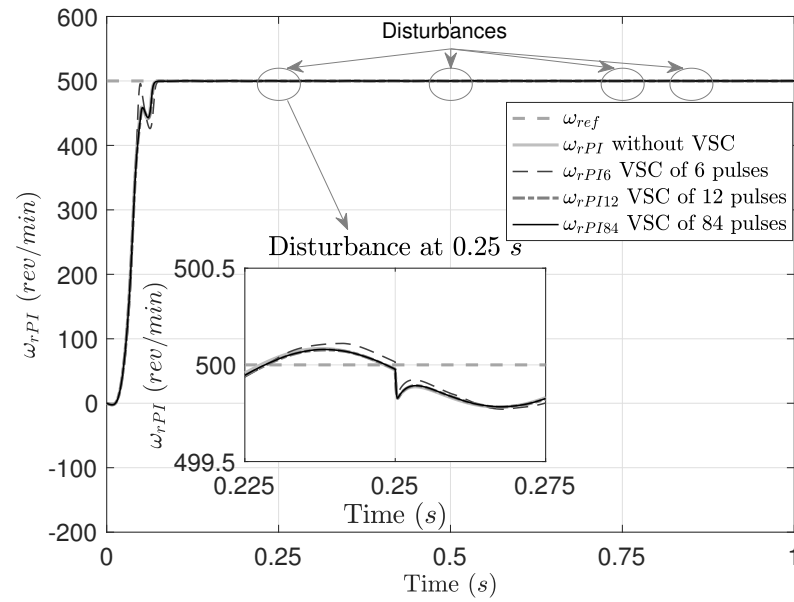


Figure 10. Velocity tracking performance for the squirrel-cage induction motor without VSC and with VSCs of 6, 12, and 84 pulses using the PI control algorithm.

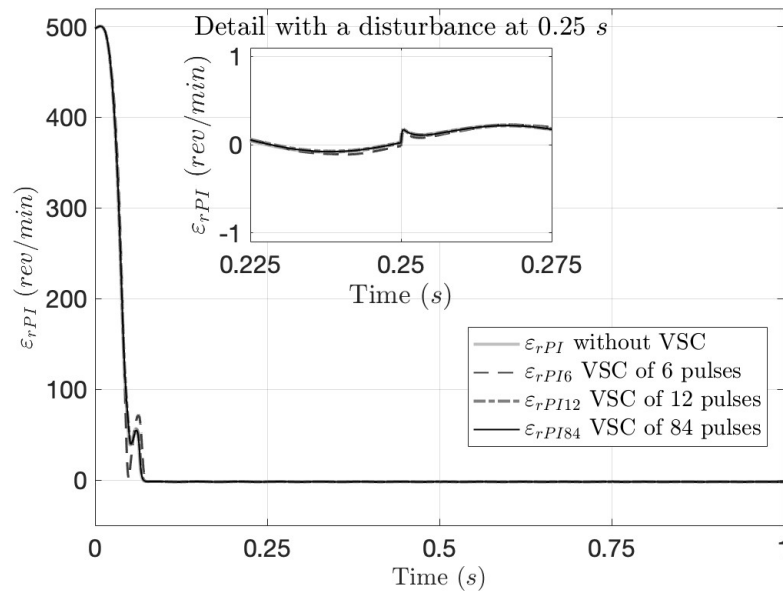


Figure 11. Tracking errors for the squirrel cage induction motor without VSC and with VSCs of 6, 12, and 84 pulses using the PI control algorithm.

Figures 12 and 13 depict the control input voltages $v_{\alpha sPI}$ and $v_{\beta sPI}$, respectively, for systems without VSC and with VSCs of 6, 12, and 84 pulses. The inputs are bounded to obtain feasible simulation results with the PI control algorithm. In both figures, a detail in 0.25 s when the external disturbance T_L changes from 4 to 12 N · m are displayed. At this time, all the voltages change suddenly to the bound value. This means that with the PI controller, the system requires a big input signal.

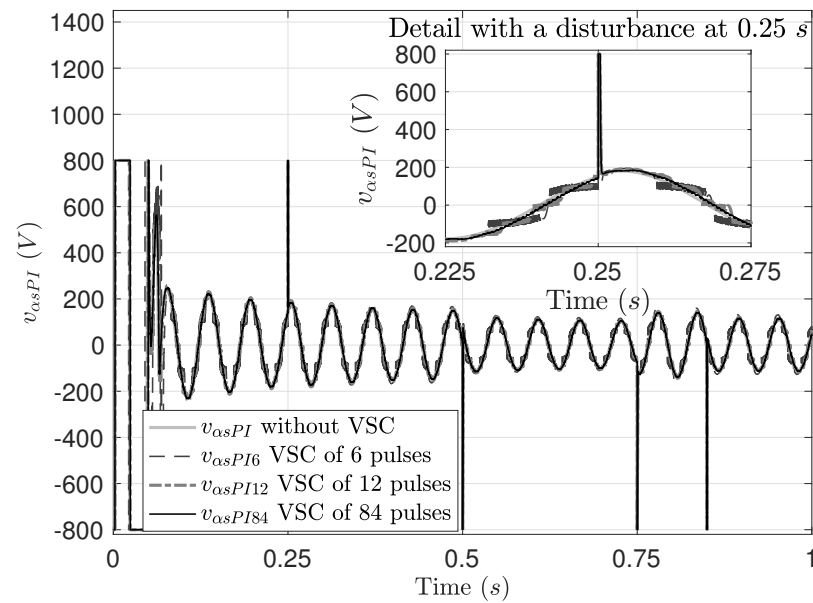


Figure 12. Control input performance $v_{\alpha sPI}$ using the PI control algorithm.

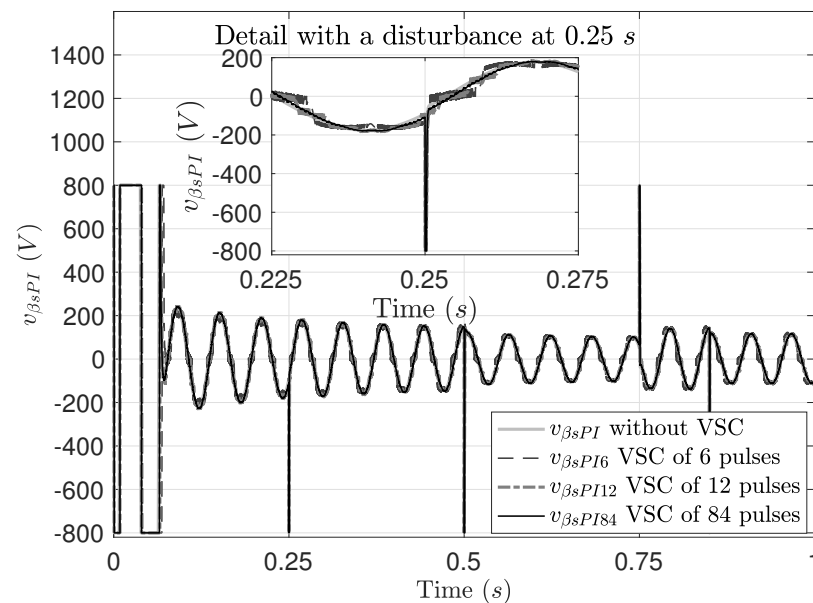


Figure 13. Control input performance $v_{\beta sPI}$ using the PI control algorithm.

In order to contrast the behavior of the system with the SM control and the bounded PI control in terms of energy, the same conditions are considered, which means a load that requires a constant velocity of 500 rev/min, an idle induction motor with the parameters of Table 1, and the torque variations shown in Figure 2. The used energy profile of the motor is portrayed in Figure 14. A very large transitory is needed to ensure the performance of the motor, but after around 0.1 s the behaviors of the system with and without VSCs are very close to each other. Figure 15 depicts the energy profile after the motor startup and the disturbances take place. The required energy is very similar without and with any VSC using this type of controller. The energy consumption is also indicated in Table 3. The frequency of the steady-state signal required for the system to function is slightly lower than for the SM system, with 17.52848 Hz, with a maximum voltage of 110.032 V and 80.1119 V_{RMS} , which constitutes a voltage around two times of that required with the SM system. The variations are illustrated in Figure 16. A big peak can be noticed in this figure,

and several fast commutations on the 6 and 12 pulses VSCs are also evident. The THD increases due to the found peak, and the values are 4.56%, 5.41%, 18.27%, and 47.04% for outputs without VSC, 84, 12, and 6 pulses, respectively. This confirms the fact that when using a 84-pulse VSC, the harmonic content produced by the power electronics device is minimum.

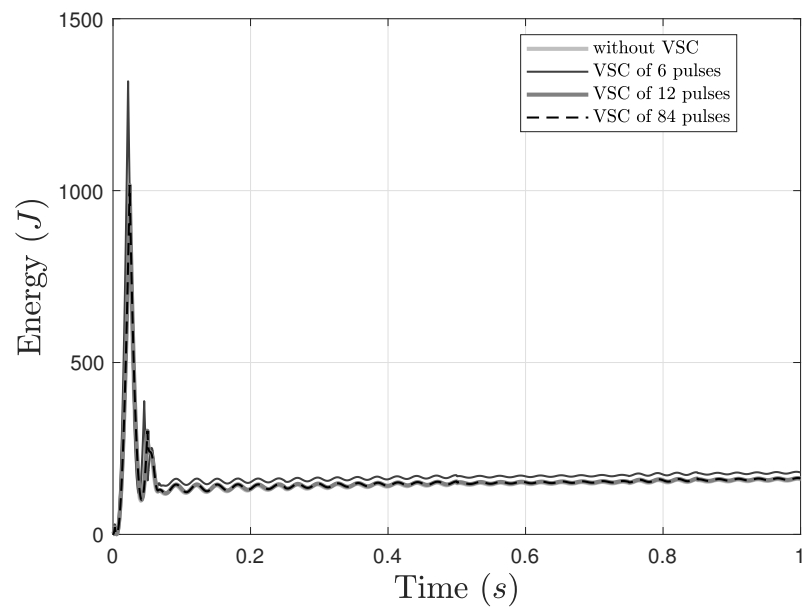


Figure 14. Energy profile for the squirrel cage induction motor without VSC and with VSCs of 6, 12, and 84 pulses using the PI control algorithm.

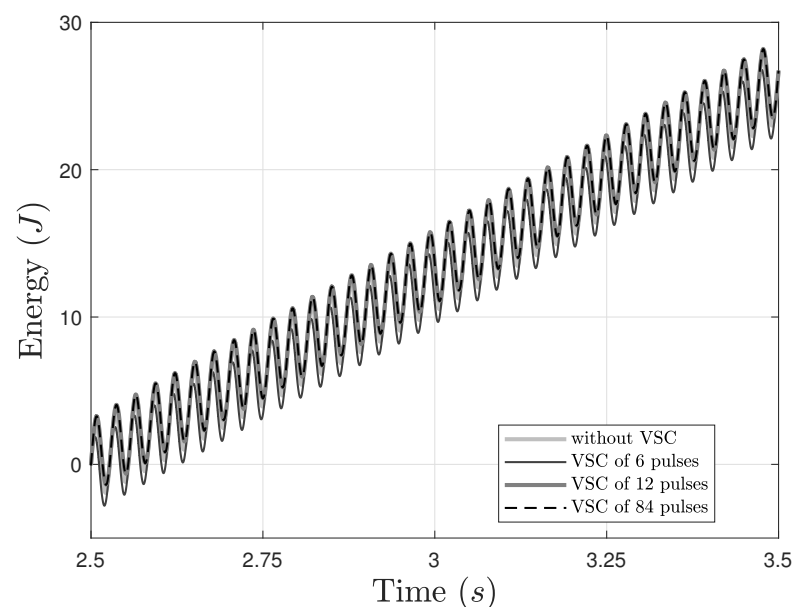


Figure 15. Energy profile for the squirrel cage induction motor without VSC and with VSCs of 6, 12, and 84 pulses, after torque variations using the PI control algorithm.

Table 2 shows the dynamic and steady-state analysis for the velocity tracking performance, where the first column represents the time when the external disturbance occurs and the value of this changed; the second column is the statistical parameter that is evaluated; columns 3 and 4 correspond to the values obtained for the system without VSC (SM and PI, respectively); columns 5 (SM) and 6 (PI) correspond to a system with VSC of 6 pulses;

columns 7 (SM) and 8 (PI) correspond to a system with VSC of 12 pulses; and columns 9 (SM) and 10 (PI) correspond to a system with VSC of 84 pulses.

Table 3. The energy used for the startup and torque variations period (2.5 s).

VSC Type	Time = 0.2 s (J)	%	Time = 0.2 s (J)	%
without VSC	1206.76	100	1506.81	100
84 pulses	1128.25	93.49	1428.46	94.80
12 pulses	1129.36	93.59	1468.68	97.47
6 pulses	2649.87	219.59	3047.86	202.27

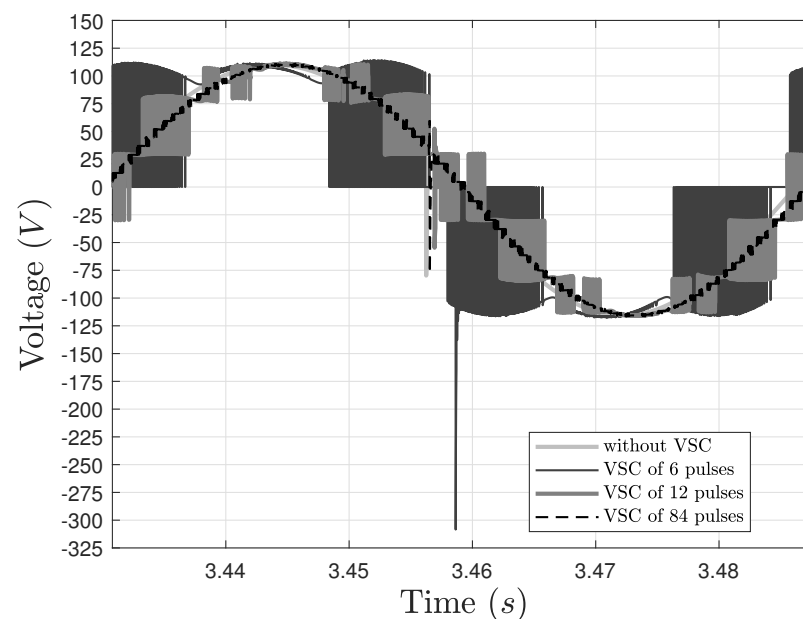


Figure 16. Steady state voltage without VSC and with VSCs of 6, 12, and 84 pulses using the PI control algorithm.

In addition, in each row, the minimum parameter is light-cooper highlighted (for the case of the SM with the equivalent control) and highlighted in gray (for the case of the PI controller). As can be seen in this table, almost all the minimum values for the SM controller correspond to the plant with the VSC of 84 pulses as the driver. Note that the minimum values are compared only for the plants with VSC, because the plant without VSC is the reference of the optimal value. Additionally, for the case of the PI controller, all the minimum values correspond to the system with the VSC of 84 pulses. The results presented in this table confirm the effectiveness of the VSC of 84 pulses in almost all of the comparisons. An exception to this comparison constitutes the M_p in the VSC of 6 pulses for the SM controller. This behavior is at the beginning of the simulation and we attribute this result to the fact that the startup of the motor requires a quasi-constant voltage at the beginning, which is easier to attain with a 6-pulse converter. However, the settling time is higher compared to using one of the other converters, which demonstrates the superior quality of the VSC with a higher number of pulses. Now, by making a comparison between the results of SM with PI in the RMS error without VSC and with 6 and 12 pulses, one can observe that the values of the PI are lower than the SM in almost all of these comparisons. Regarding the M_p in the sudden changes of the external disturbance, the PI shows lower values than SM. In this work, although the comparison between the performance of the controllers was not the main objective, the results show that the PI performs slightly better than SM, which indicates the precision that is had when tuning the PI controllers to constant reference velocity signals. Of course, there could be other scenarios of comparison, such as

varying the reference velocity with time-varying signals. However, to compare these and other scenarios is out of the scope of this paper.

In order to verify steady-state energy consumption, (after the settling time is reached for the last modification on the torque), 2.5 s was considered sufficient to compute the total energy that is depleted. The amount needed for the ideal voltage source is 1506.81 J, considered 100% for analysis. The amount of energy used when VSCs are part of the system is presented in Table 3. After this time, we can consider the steady-state on the system and the needed energy profile is illustrated in Figure 8.

6. Conclusions

This research has presented how two control strategies used for a defined task are affected by the quality of the signals provided by power electronics converters. The side effects of not using low THD converters include high oscillations around the reference, large power demand when starting up, an important increase of the energy consumption in steady-state, and, in extreme cases, the use of very sophisticated control strategies.

By combining a good control strategy, which in this case is the sliding mode with an equivalent control or the PI control algorithm, with a high-quality voltage source converter, allows applications, in general, to perform very close to the established plan, which for this case is the obtained signals without VSC. The signals achieved using the plant with VSC, 16, 12 and 64 pulses could be reached.

7. Discussion

This work presents the simulation results for controlling the angular speed of the squirrel-cage induction motor model, even when the system has two controlled outputs: the angular speed and the square modulus of rotor flux linkages [14]. The reason for showing only these results is that the main contribution of the work is to show the advantages of applying a VSC of 84 pulses over the use of VSC of 6 and 12 pulses.

Author Contributions: Methodology, C.E.C. and A.V.-G.; Software, C.E.C. and A.V.-G.; Validation, C.E.C., A.V.-G. and O.A.M.; Formal analysis, C.E.C. and A.V.-G.; Investigation, C.E.C., A.V.-G. and O.A.M.; Resources, C.E.C.; Visualization, H.A.G. and O.A.M.; Supervision, H.A.G. All authors have read and agreed to the published version of the manuscript.

Funding: The authors would like to thank Universidad Panamericana, for their support through the program “Fomento a la Investigación UP 2022”, and project “Estudio de topologías de convertidores de cd-cd” UP-CI-2022-GDL-06-ING.

Data Availability Statement: Not applicable.

Acknowledgments: The authors gratefully acknowledge the support of Universidad Panamericana Campus Guadalajara, and Universidad de Guadalajara, Jalisco, México.

Conflicts of Interest: The authors declare no conflict of interest.

Abbreviations

The following abbreviations and variables are used in this manuscript:

Acronym	Name
AC	Analog current
DC	Direct current
MPCC	Model predictive current control
PI	Proportional-Integral
THD	Total harmonic distortion
VSC	Voltage source converter

Variable	Name
ω_m	Angular velocity
ω_{ref}	Reference angular velocity
$\lambda_{\alpha r}, \lambda_{\beta r}$	Rotor flux linkages at α and β axis
$i_{\alpha s}, i_{\beta s}$	Stator currents at α and β axis
$v_{\alpha s}, v_{\beta s}$	Voltages in stationary reference frame α and β
$\mathbf{v}_s = \begin{bmatrix} v_{\alpha} & v_{\beta} \end{bmatrix}^T$	Stator vector voltages α and β
ϕ_r	Rotor flux linkages
ϕ_{ref}	Reference rotor flux linkages
$\mathbf{i}_s = \begin{bmatrix} i_{\alpha s} & i_{\beta s} \end{bmatrix}^T$	Stator vector currents
\mathbf{i}_{ref}	Reference stator vector currents
$\boldsymbol{\varepsilon}_1 = \begin{bmatrix} \omega_{ref} - \omega_m \\ \phi_{ref} - \phi_r \end{bmatrix}$	Tracking error vector 1
$\boldsymbol{\varepsilon}_2 = \begin{bmatrix} \mathbf{i}_{ref} - \mathbf{i}_s \end{bmatrix}$	Tracking error vector 2
$\mathbf{s} = \boldsymbol{\varepsilon}_2 = \mathbf{i}_{ref} - \mathbf{i}_s$	Sliding manifold
\mathbf{u}	Sliding modes with equivalent control law
\mathbf{u}_{eq}	Equivalent control law
\mathbf{u}_{max}	Maximum voltage given by the source
T_L	Load torque

References

- He, H.; Liu, B.; Wang, Q.; Tan, F.; Gui, H.; Zhang, C. Active Disturbance Rejection Control-Based Robust Model Predictive Current Control for Induction Motor. *J. Electr. Eng. Technol.* **2022**, *17*, 3413–3425. [\[CrossRef\]](#)
- Mousavi, M.S.; Davari, S.A.; Nekoukar, V.; Garcia, C.; He, L.; Wang, F.; Rodriguez, J. Predictive torque control of induction motor based on a robust integral sliding mode observer. *IEEE Trans. Ind. Electron.* **2022**, *70*, 2339–2350. [\[CrossRef\]](#)
- Wang, T.; Wang, B.; Yu, Y.; Xu, D. Fast High-Order Terminal Sliding-Mode Current Controller for Disturbance Compensation and Rapid Convergence in Induction Motor Drives. *IEEE Trans. Power Electron.* **2023**. [\[CrossRef\]](#)
- Wang, B.; Wang, T.; Yu, Y.; Xu, D. Second-Order Terminal Sliding-Mode Speed Controller for Induction Motor Drives with Nonlinear Control Gain. *IEEE Trans. Ind. Electron.* **2022**, *70*, 10923–10934. [\[CrossRef\]](#)
- Lumertz, M.; dos Santos, S.; Guazzelli, P.; de Oliveira, C.; de Aguiar, M.; Monteiro, J. Performance-based design of pseudo-sliding mode speed control for electrical motor drives. *Control Eng. Pract.* **2023**, *132*, 105413. [\[CrossRef\]](#)
- Nguyen-Vinh, Q.; Pham-Tran-Bich, T. Sliding mode control of induction motor with fuzzy logic observer. *Electr. Eng.* **2023**. Advance online publication. [\[CrossRef\]](#)
- Accetta, A.; Alonge, F.; Cirrincione, M.; D'Ippolito, F.; Pucci, M.; Rabbeni, R.; Sferlazza, A. Robust control for high performance induction motor drives based on partial state-feedback linearization. *IEEE Trans. Ind. Appl.* **2018**, *55*, 490–503. [\[CrossRef\]](#)
- Mengoni, M.; Zarri, L.; Tani, A.; Serra, G.; Casadei, D. A comparison of four robust control schemes for field-weakening operation of induction motors. *IEEE Trans. Power Electron.* **2011**, *27*, 307–320. [\[CrossRef\]](#)
- Pohl, L.; Vesely, I. Speed control of induction motor using H_{∞} linear parameter varying controller. *IFAC-PapersOnLine* **2016**, *49*, 74–79. [\[CrossRef\]](#)
- Ammar, A.; Talbi, B.; Ameid, T.; Azzoug, Y.; Kerrache, A. Predictive direct torque control with reduced ripples for induction motor drive based on T-S fuzzy speed controller. *Asian J. Control* **2019**, *21*, 2155–2166. [\[CrossRef\]](#)
- Beltran-Carbajal, F.; Tapia-Olvera, R.; Valderrabano-Gonzalez, A.; Lopez-Garcia, I. Adaptive neuronal induction motor control with an 84-pulse voltage source converter. *Asian J. Control* **2021**, *23*, 1603–1616. [\[CrossRef\]](#)
- Utkin, V.; Guldner, J.; Shi, J. *Sliding Mode Control in Electro-Mechanical Systems*; CRC Press: Boca Raton, FL, USA, 2017.
- Utkin, V.I.; Poznyak, A.S. Adaptive sliding mode control with application to super-twist algorithm: Equivalent control method. *Automatica* **2013**, *49*, 39–47. [\[CrossRef\]](#)
- Morfin, O.A.; Valenzuela, F.A.; Betancour, R.R.; Castañeda, C.E.; Ruiz-Cruz, R.; Valderrabano-Gonzalez, A. Real-time SOSM super-twisting combined with block control for regulating induction motor velocity. *IEEE Access* **2018**, *6*, 25898–25907. [\[CrossRef\]](#)
- Morfin, O.A.; Ruiz-Cruz, R.; Hernández, J.I.; Castañeda, C.E.; Ramírez-Betancour, R.; Valenzuela-Murillo, F.A. Real-Time Sensorless Robust Velocity Controller Applied to a DC-motor for Emulating a Wind Turbine. *Energies* **2021**, *14*, 868. [\[CrossRef\]](#)
- Liu, Y.; Arrillaga, J.; Watson, N. Reinjection concept: A new option for large power and high-quality AC–DC conversion. *IET Power Electron.* **2008**, *1*, 4–13. [\[CrossRef\]](#)
- Najafpour, S.; Ghandehari, R. Harmonic Reduction by Voltage Reinjection Strategy in 12-Pulse VSI for High Power Applications. In Proceedings of the 2021 12th Power Electronics, Drive Systems, and Technologies Conference (PEDSTC), Tabriz, Iran, 2–4 February 2021; pp. 1–6.
- Valderrabano-Gonzalez, A.; Ramirez, J.M.; Tapia-Olvera, R.; Rosas-Caro, J.C.; Lozano-Garcia, J.M.; Gonzalez-Lopez, J.M. Analysis and Implementation of an 84-Pulse STATCOM. In *Static Compensators (STATCOMs) in Power Systems*; Springer: Singapore, 2015; pp. 83–110.

19. *IEEE. 519-2014*; IEEE Recommended Practice and Requirements for Harmonic Control in Electric Power Systems. Revision of IEEE Std 519-1992. IEEE: Piscataway, NJ, USA, 2014; pp. 1–29.
20. *IEEE. 1159-2019*; IEEE Recommended Practice for Monitoring Electric Power Quality. Revision of IEEE Std 1159-2009. IEEE: Piscataway, NJ, USA, 2019; pp. 1–98.
21. Valderrabano-Gonzalez, A.; Beltran-Carbajal, F.; Tapia-Olvera, R.; Aguilar-Mejia, O.; Rosas-Caro, J. Design methodology for interfacing DERs to power systems through VSC. *Math. Probl. Eng.* **2021**, *2021*, 5541375. [[CrossRef](#)]
22. Morfín, O.A.; Castañeda, C.E.; Ruiz-Cruz, R.; Valenzuela, F.A.; Murillo, M.A.; Quezada, A.E.; Padilla, N. The squirrel-cage induction motor model and its parameter identification via steady and dynamic tests. *Electr. Power Components Syst.* **2018**, *46*, 302–315. [[CrossRef](#)]
23. Loukianov, A.G. Robust block decomposition sliding mode control design. *Math. Probl. Eng.* **2003**, *8*, 349–365. [[CrossRef](#)]
24. Krause, P.C.; Wasynczuk, O.; Sudhoff, S.D.; Pekarek, S.D. *Analysis of Electric Machinery and Drive Systems*; John Wiley & Sons: Hoboken, NJ, USA, 2013; Volume 75.

Disclaimer/Publisher’s Note: The statements, opinions and data contained in all publications are solely those of the individual author(s) and contributor(s) and not of MDPI and/or the editor(s). MDPI and/or the editor(s) disclaim responsibility for any injury to people or property resulting from any ideas, methods, instructions or products referred to in the content.